AIAA 82-4094

Multistable Vortex Patterns on Slender, Circular Bodies at High Incidence

Andrew B. Wardlaw Jr.* and William J. Yanta*
Naval Surface Weapons Center, Silver Spring, Md.

A rigidly supported tangent ogive model has been tested in low turbulent, incompressible flow at incidences of 35, 45, and 55 deg. A constant streamwise Reynolds number of 1.5×10^5 was maintained that produced laminar boundary-layer separation. Both unsteady pressures and flowfield velocities were measured, the latter with a three component laser Doppler velocimeter. Analysis of the results indicates that the vortex pattern may be unsteady at times, but that the flowfield can be idealized as steady and that variations in the measured side force are principally a result of changes in the mean vortex pattern. Large side forces are shown to be induced by flowfields that shed a major part of the first vortex. A relationship is established between side force magnitude and surface pressure fluctuations. The repeatability of side force measurements is examined and tests featuring high side force levels are found to be the most reproducible. Tests on a blunted model produced a decrease in side force and body vortices that were located a greater distance from the model surface. Comparison of current results with those from other studies suggests that a unique flowfield is associated with each side force value. In the incidence range of 45-55 deg, peak local force values from different sources are also in good agreement.

Nomenclature

C_{dc} = $F_N/(Dq\sin^2\alpha)$
$\bar{C}_p$ = average value of $(p-p_\infty)/(q\sin^2\alpha)$ for 200 data points taken at each visit to a pressure tap
C_y = $F_y/(Dq\sin^2\alpha)$
$C_{y\,\text{peak}}$ = maximum C_y value
D = model diameter, 5.67 cm
F_N = normal force per unit length
F_y = side force per unit length
q = freestream dynamic pressure
Re_s = Reynolds number based on freestream properties and $D/\sin\alpha$
U_∞ = freestream velocity
u,v,w = Cartesian velocity components
x,y,z = Cartesian coordinates (see Fig. 1)
x' = distance along model axis measured from nose tip
α = angle of attack
Γ = circulation, m^2/s
σ_{c_p} = standard deviation of C_p for the 200 data points taken at each visit to a tap
$\bar{\sigma}_{c_p}$ = average σ_{c_p} at a specific axial station
Φ = model roll orientation
ϕ = circumferential angle; windward is $\phi = 180$ deg
ω = [Γ/unit area] $D/(\pi U_\infty \sin\alpha)$

I. Introduction

INCREASED performance requirements have made it necessary for missiles to fly at large angles of attack. At incidences greater than a few degrees, the flow separates from the leeside of the body rolling up to form a pair of symmetric vortices. With increasing angle of attack the shed vortices form a nominally steady and asymmetric pattern, even on axisymmetric bodies. Unfortunately, lack of repeatability has plagued studies of asymmetric vortices and it has not been possible experimentally to quantitatively define the flowfield, surface pressure distributions, or resulting aerodynamic coefficients. Most strongly affected is the degree of asymmetry in the pressure distribution and the resulting yaw plane loads. Both of these quantities vary with changes in the roll orientation of axisymmetric models.

A large number of experimental studies on the high angle-of-attack flowfield have been reported in the literature.[1-17] Until recently it was often presumed that the flowfield was steady and, generally, only average values were measured. Interest in the unsteady aspects of the high angle-of-attack flowfield was stimulated by Lamont and Hunt[18,19] who hypothesized that flow unsteadiness, possibly triggered by freestream turbulence, might be the principal cause of experimental nonrepeatability. Additional studies have become available recently which measured standard deviation as well as average value of various flowfield quantities.[15-17] In Ref. 16 the authors presented laser Doppler velocimeter (LDV) and surface pressure data on a tangent ogive model which included standard deviation and average values of both pressure and velocity components. An examination of these results indicates that large velocity fluctuations occur in portions of the flowfield featuring high levels of vorticity and that body surface areas adjacent to these regions experience high levels of pressure fluctuation. Comparison of velocity and pressure data shows that the peak side force level forms as the first vortex is shed and is caused by the large suction imparted to the ogive body by the remaining vortex. Nonrepeatability in side force appears principally due to changes in the mean flowfield pattern. However, some vortex unsteadiness, particularly far from the nose, is postulated to occur.

The current paper reports on an extension to the work of Ref. 16 using essentially the same test apparatus. In the present study the objective is to determine the link between varying side force levels and flowfield structure. To achieve varying side force levels, both a sharp tipped and slightly blunted tangent ogive model are tested at a large number of different roll angles. Flowfield surveys are taken at roll angles featuring maximum and minimum side forces.

The model, instrumentation, and testing procedure are described in Sec. II and the data taken are presented in Sec. III. These results describe flowfield fluctuations, the relation between side force and vortex structure, and side force variation as a function of model roll angle. A discussion of results is provided in Sec. IV and conclusions are summarized in Sec. V.

II. Description of the Model and Experiment

The experimental model shown in Fig. 1, was a 5.67-cm-diam tangent ogive with a nose fineness of 3 and an afterbody length of 9.6 calibers. The sharp nose tip could be unscrewed

Received March 12, 1981; revision received Aug. 10, 1981. This paper is declared a work of the U. S. Government and therefore is in the public domain.

*Aerospace Engineer. Associate Fellow AIAA.

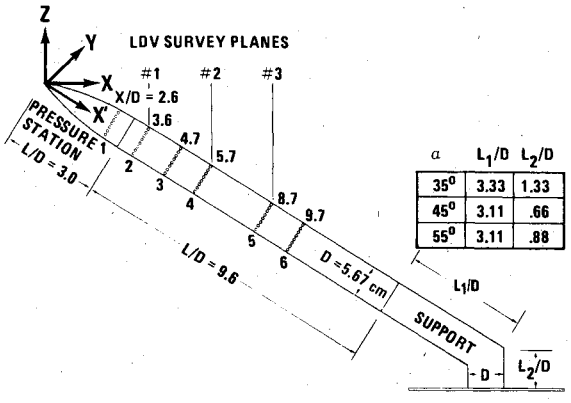

Fig. 1 Tangent ogive pressure model and support system. The rows of small circles indicate the locations of pressure measuring stations.

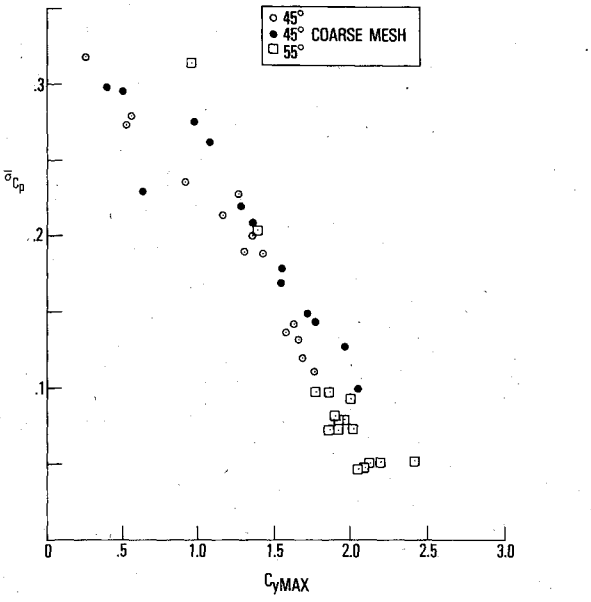

Fig. 2 Circumferential pressure profile. The symbols represent the average pressure while the vertical lines are indicative of the standard deviation.

and replaced with a 10% blunted (spherical) nose tip. Six cross-sectional stations were each instrumented with 24 pressure taps located circumferentially at intervals of 15 deg. Pressures were monitored using three internally mounted ±0.7 kPa (±0.1 psi) Setra differential pressure transducers. Each of these devices was connected to a 48 port internally mounted Scanivalve allowing all 144 pressure taps to be sampled. Pretest calibrations indicated that pressure fluctuations on the order of 500 Hz could be measured. A recently developed three component LDV, described in Ref. 20, was used to survey the leeward flowfield structure in the manner outlined in Ref. 16. As shown in Fig. 1, the three survey planes were perpendicular to the freestream direction.

The model was tested in the U. S. Naval Academy's 1×1.3-m wind tunnel. The nominal freestream turbulence level in the streamwise direction was 0.1%. The wind-tunnel velocity was set at 20, 24, 29 m/s at incidences of 35, 45, and 55 deg, respectively, insuring a streamwise Reynolds number of 1.5×10^5. A coarse mesh with 3.175-mm wire diameter and 55% porosity was inserted in the wind tunnel in certain tests increasing stream turbulence levels to a nominal 2%. The sharp nosed model was tested at the incidences of 35, 45, and 55 deg while the blunted one was tested only at $\alpha = 45$ and 55 deg. A single test series was run with the coarse mesh in place. These experiments featured the sharp model at an incidence of 45 deg.

At each angle of attack, pressure only tests were initially made at $\Phi = 0$ deg and the collected data were reduced and integrated on line to determine normal and side forces. The wind tunnel was then shut down, the roll orientation of the model was incremented by 30 deg, and another pressure only test was run. This procedure was repeated until the model had been rotated completely. The model was then positioned in turn to the roll angles producing the maximum and minimum side force and the flowfield was probed using the LDV system.

The pressure alone tests took about 10 min to complete. The pressure taps were sampled three at a time until the entire model surface had been surveyed. At each pressure tap 200 pressure measurements were recorded which took about 10 s. Tests in which LDV and pressure data were acquired spanned several hours. The traverse plane was mapped point by point and at each position 200 LDV measurements were taken generally in less than a minute. The data acquisition system was controlled by the LDV system. Each time a velocity measurement was acquired, a pressure data point at each of the taps being sampled was recorded.

A sufficient number of flowfield points were probed during each run to complete a map of a single traverse plane. On the forward plane about 100 points were measured, while on the aft plane the necessary number increased to nearly 200. Since each Scanivalve was connected to 48 ports this resulted in repeat visits to the same pressure tap.

An examination of the circumferential pressure profiles indicated that a laminar boundary-layer separation occurred in all runs. This was determined by comparing pressure profiles taken during the current study with those measured on inclined cylinders. This point is discussed further in Ref. 16.

III. Experimental Results

Fluctuation of Measured Quantities

The pressure standard deviation σ_{c_p}, which is calculated from the 200 data points acquired at each visit to a pressure tap, is a measure of the relatively high frequency flowfield fluctuations. Comparison of $\bar{C}_p$ from repeat visits to the same port provides an indication of the longer term variations that are probably attributable to changes in the mean vortex pattern. Examination of the pressure data collected during the LDV runs indicated that in many tests $\bar{C}_p$ values accurately repeated during a test implying the existence of a steady vortex pattern. This was particularly true for the blunted model which exhibited low side forces at both of the tested incidences. This situation also occurred for some of the runs on the sharp model at angles of attack of 45 and 55 deg where high side force levels are attained. In other runs, $\bar{C}_p$ did not repeat as well which suggests a meandering of the vortex pattern during the test. In one run the pressure profile changed dramatically during the experiment indicating that the vortex pattern switched from an asymmetric to a nearly symmetric pattern.[21]

An examination of the pressure data from all runs indicates a consistent relationship between side force magnitude and σ_{c_p} values at axial stations near or upstream of the points where C_y is maximum. In Fig. 2 the pressure station featuring the maximum C_y is considered and C_y is plotted against $\bar{\sigma}_{c_p}$. The illustrated data is taken from the pressure alone sharp nose model tests at the incidences of 45 and 55 deg. Under these conditions high side force levels occur and Fig. 2 clearly indicates that $\bar{\sigma}_{c_p}$ increases as the side force decreases. Note that the measurements at $\alpha = 45$ deg with and without the turbulence generating screens in place are remarkably similar. The high turbulence tests with the screens in place showed slightly higher $\bar{\sigma}_{c_p}$ values. The individual σ_{c_p} levels are only grossly altered on the windward side of the body where the levels changed from a nominal 0.025 without the screens to 0.065 with the screens in place. The blunted model at all

incidences and the sharp model at $\alpha = 35$ deg produced very low side force levels and a clear trend relating $\bar{\sigma}_{c_p}$ to the local side force magnitude is not evident.

Flowfield Development Corresponding to Different Side Force Levels

The pressure alone tests produced a wide range in side force as the model was rotated completely. The $\bar{C}_p$ distributions at the pressure station 4 are shown in Fig. 3 for tests carried out at an incidence of 45 deg. For $\alpha = 45$ deg and with the screens removed from the tunnel the side force maximum always occurred at the forth pressure station. Included are the measurements from the roll orientations producing the maximum and minimum side force and data from a blunted model run that produced no measurable side force. The symmetric pressure profiles shown in Fig. 3 are typical of those that form near the model nose or along the entire model length in cases featuring low side forces. Here the pressure profiles exhibit minimums windward of the model shoulder that are relatively symmetric in both location and magnitude. On the leeward plane, which is presumably at or very close to the rear stagnation point, a local $\bar{C}_p$ maximum and σ_{c_p} minimum occur.

At roll orientations that produce a large side force a higher pressure develops on the side of the model from which the vortex is shed. The pressure minimums windward of the model shoulder become asymmetrically disposed at axial locations exhibiting a large side force as is shown in Fig. 3. The minimum pressure on the low pressure side of the model decreases while the minimum pressure on the high pressure side increases and its location moves windward. Near the leeward meridian a steep pressure gradient develops bridging the pressure level on one side of the model to that on the other. Near the center of this gradient the maximum σ_{c_p} value occurs. The traverse plane velocity vectors shown in Fig. 4a indicate that the rear stagnation point moves toward the high pressure side of the bridging pressure gradient.

The flowfields and pressure distributions associated with high, moderate, and low side force levels are contrasted in Fig. 4. The illustrated data were taken near the axial station where the maximum local side force occurs. The low side force data is from a run with the turbulence screens inserted in the wind tunnel. However, this change in experimental procedure does not appear to have altered the structure of the flowfield. The pressure profiles shown in Fig. 4 are in the crossflow plane which is perpendicular to the model axis while the plane of the flowfield survey is perpendicular to the freestream direction. The flowfield velocity vectors clearly denote three different vortex patterns, each with its own level of asymmetry. Examination of the data presented in Fig. 4 indicates that the highest side force level is associated with the most asymmetric flowfield. In the case illustrated in Fig. 4a the entire right-hand vortex has been shed. The flowfield associated with a low side force level is shown in Fig. 4c and appears to be nearly symmetric. Figure 4 clearly shows that the largest side forces are generated by vortex patterns which are the most asymmetric.

The flowfield and constant vorticity contours generated by the blunted model are shown in Fig. 5. A comparison of Figs. 4c and 5 indicates that the vortex generated by the blunted model is further from the model surface. In other respects the flowfields are very similar. An integration of the measured vorticity over the surveyed portion of the flowfield produces

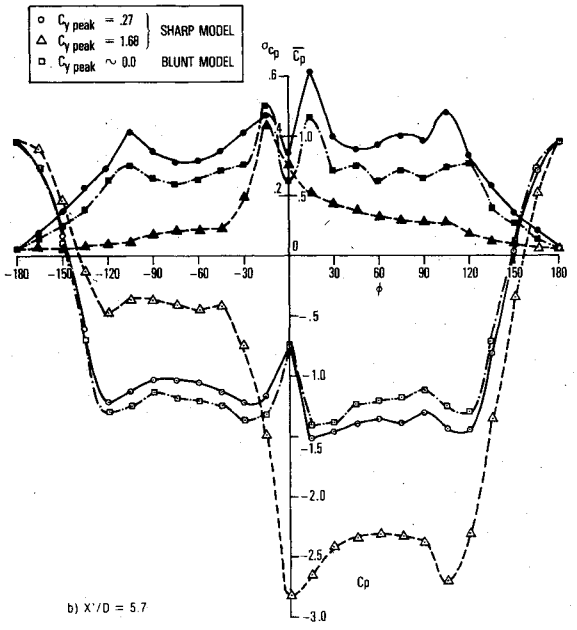

Fig. 3 $\bar{\sigma}_{c_p}$ as a function of C_y at the axial station featuring the maximum C_y. Open symbols indicate $\bar{C}_p$, solid ones represent σ_{c_p}.

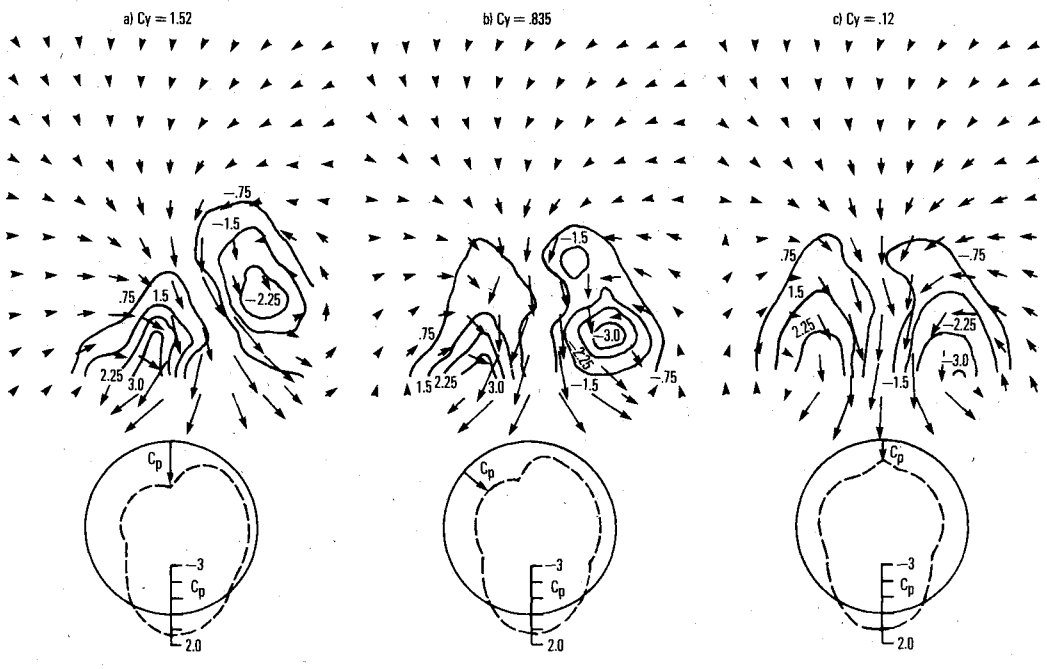

Fig. 4 The flowfield survey at traverse plane 2 and $\bar{C}_p$ distribution at $X'/D = 5.7$ for the sharp model at $\alpha = 45$ deg. The circle represents the outline of the model in the crossflow plane while the solid lines in the flowfield indicate constant vorticity contours (ω). The distance between the dashed line and the model surface is a measure of $\bar{C}_p$ with positive values being located outside the circle and negative ones inside.

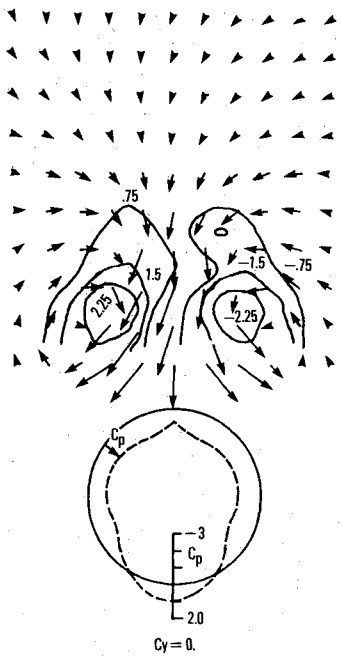

Fig. 5 The flowfield survey at traverse plane 2 and the $\bar{C}_p$ distribution at $X'/D = 5.7$ for the blunted model at $\alpha = 45$ deg. The circle represents the outline of the model. The lines in the flowfield are constant vorticity (ω) contours. The distance between the dashed line and the model surface is a measure of $\bar{C}_p$ with positive values being located outside the circle and negative ones inside.

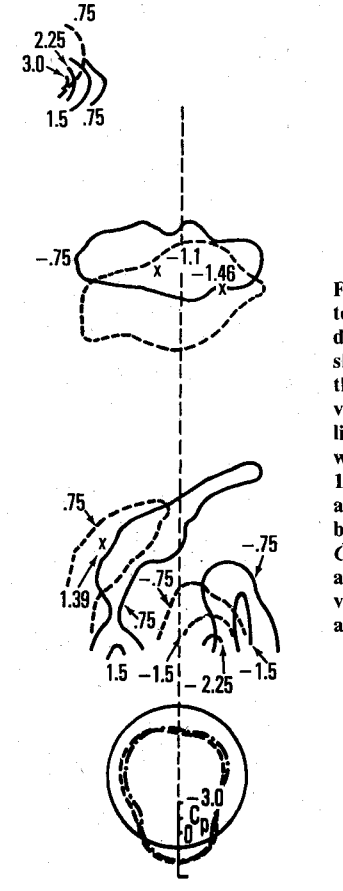

Fig. 6 Constant vorticity contours in traverse plane 3 and $\bar{C}_p$ distribution at $X'/D = 8.7$ on the sharp model at $\alpha = 55$ deg. Lines in the flowfield represent constant vorticity contours (ω). The dotted lines are current results ($C_y = 0.5$) while the solid ones are from Ref. 16 ($C_y = 0.12$). The dashed (- -) and dotted (- · -) lines near the body represent the magnitude of $\bar{C}_p$ measured in the current study and Ref. 16, respectively. Positive values are located outside the circle and negative ones inside.

nearly identical vortex strengths. The traverse plane velocity vectors are relatively symmetrically disposed in both cases, particularly near the model surface.

At an incidence of 35 deg the flowfield did not become highly asymmetric and the symmetric pressure profiles of Fig. 3 were often observed along the entire model length. At the roll orientation featuring the largest side forces, which were on the order of $C_{y\,max} = 0.5$, the pressure distribution became asymmetric in the manner of Fig. 3, but the $\bar{C}_p$ difference between the two sides of the model remained small.

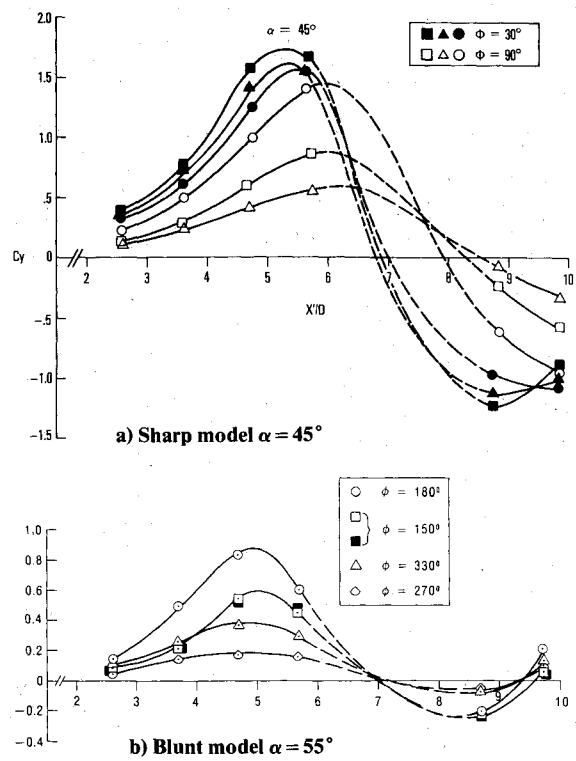

Fig. 7 C_y distribution at roll orientations producing high and low side force levels.

At an incidence of 55 deg the flowfield was usually asymmetric and large side forces were produced. The maximum side force most often occurred at the first or second pressure station. In a few cases the maximum side force was located at pressure station 3 and the first pressure station exhibited a pressure profile similar to the symmetric ones in Fig. 3. The pressure station featuring $C_{y\,max}$ always had a pressure profile similar to the asymmetric one of Fig. 3. The flowfield was surveyed once on traverse planes 1 and 3. The survey taken at the first plane contained a highly asymmetric vortex pattern which was in the process of shedding the right-hand vortex. This pattern is very similar to one shown in Ref. 16 and is not repeated here.

The constant vorticity contours measured on traverse plane 3 and the pressure profiles measured at ring 5 at $\alpha = 55$ deg are given in Fig. 6. Also shown are similar data taken from Ref. 16 using the same model and testing conditions, but different roll angle. The side force magnitudes are small in both cases but substantially different. In the higher side force case the flowfield close to the model surface contains a more asymmetric vortex pattern. The difference between peak vortex strengths is larger and the regions of peak vorticity are more asymmetrically located. The increased flowfield asymmetries produce a larger pressure profile asymmetry and, hence, side force. This is consistent with the data shown in Fig. 4 which clearly features increases in pressure profile asymmetries in tests with greater flowfield asymmetries.

Side Force Measurement

Repeat side force measurements are shown in Fig. 7a for the sharp model at an incidence of 45 deg. The solid and open symbols represent data taken at roll angles that produce maximum and minimum side forces, respectively. The sign of C_y has been adjusted to produce a positive value near the model nose. The illustrated results include data from both the short pressure alone tests and longer LDV runs. It is evident from Fig. 7 that the most repeatable results occurred at a roll orientation featuring high side force levels. At roll angles producing low side forces, the sign of C_y often changed in

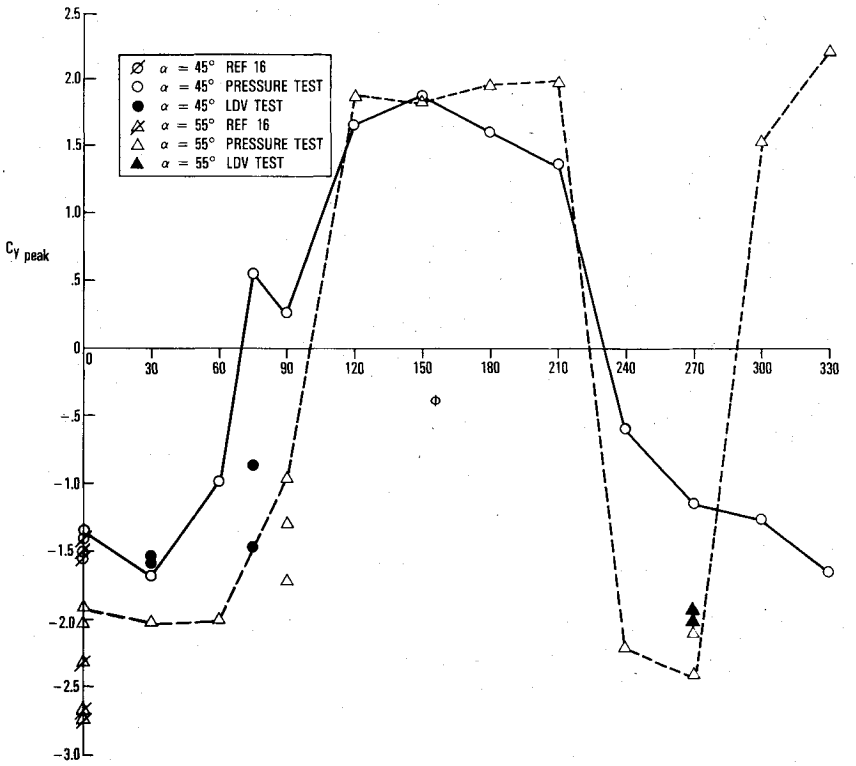

Fig. 8 $C_{y\ peak}$ **as a function of roll angle. The solid and dashed lines connect the first measurement made at each roll angle. The open and closed symbols are repeat runs from this study while the flagged points are from Ref. 16.**

repeat tests. Data at $\alpha = 35$ deg (not shown) exhibited a very low side force at all roll angles which did not repeat well. In the case of the blunted model, lower side forces were generated as is shown in Fig. 7b, but results tended to repeat well.

It can be seen from Fig. 7 that the side force distribution curve is a damped periodic function with the maximum amplitude occurring near the model nose. An analysis of the side force occurring at a large number of roll angles suggests that both the amplitude and functional form (i.e., variation with x'/D) can change. Also, there appears to be a link between the amplitude and functional form on the sharp model at an incidence of 45 deg. The location of $C_{y\ peak}$ and $C_y = 0$ points appears to move aft as the magnitude of the side force decreases. Such a relation is not evident in the case of the blunt model and the functional form of the side force distribution curve appears to be independent of the force amplitude.

The amplitude of the side force can be characterized by the magnitude of $C_{y\ peak}$. In the current study this quantity is estimated by drawing a smooth curve through the measured side force at each axial station and noting the maximum C_y value. The variation of $C_{y\ peak}$ with changes in model roll orientation is illustrated in Fig. 8 for the incidences of 45 and 55 deg. The lines in this figure connect the first measurements made at each roll angle and the remaining symbols are repeat runs. At $\alpha = 45$ deg, $C_{y\ peak}$ transitions more smoothly from positive to negative values than at an incidence of 55 deg. For a fixed roll angle the sign of C_y peak is usually the same for both incidences.

In Fig. 9 only the first measurement made at each 30-deg roll angle increment is considered and $C_{y\ peak}$ is plotted as a function of the number of observations that exceed this value. Using this figure the probability of attaining a specific side force magnitude when testing at an arbitrary roll angle can be estimated. The data of Fig. 9 applies to the sharp model with and without the turbulence screens inserted in the wind tunnel. At an incidence of 35-deg low side force values are most likely since 5 out of 12 runs produced no measurable side force. Half of the observed $C_{y\ peak}$ values at an incidence of 45

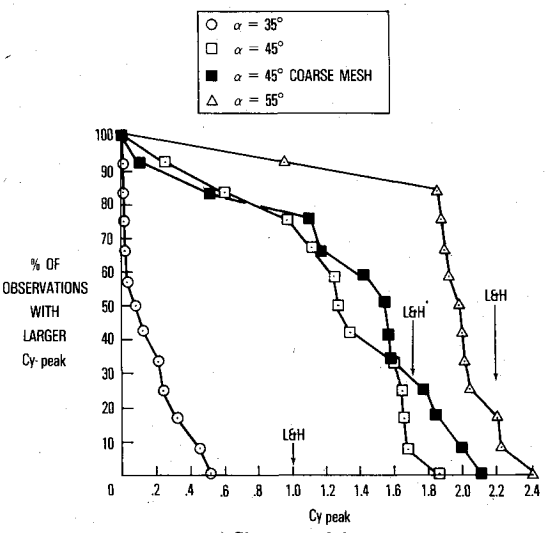

a) Sharp model

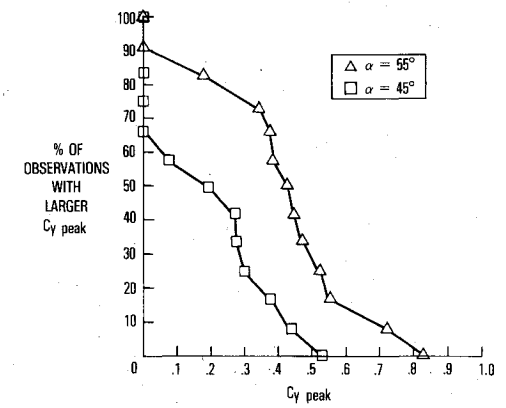

b) Blunt model

Fig. 9 $C_{y\ peak}$ **as a function of the number of roll orientations producing larger values of** $C_{y\ peak}$**. The arrows marked L&H are the maximum predicted** $C_{y\ peak}$ **values from the Lamont-Hunt correlation.**[19]

deg were greater than 70% of the maximum $C_{y\,peak}$. Insertion of the turbulence generating screens into the wind tunnel did not appear to qualitatively alter the side force distribution, however, the maximum $C_{y\,peak}$ did increase about 10%. At $\alpha = 55$ deg, most of the $C_{y\,peak}$ values are close to the maximum measured $C_{y\,peak}$ and the probability of attaining a small side force is very low. The values from the Lamont and Hunt[18] correlation for maximum $C_{y\,peak}$ are indicated in Fig. 9 and are in good agreement with the current experiment at incidences of 45 and 55 deg, but overestimate the observed $C_{y\,peak}$ at $\alpha = 35$ deg.

The blunt model $C_{y\,peak}$ distribution which is shown in Fig. 9b indicates that the likelihood of achieving a low side force level is very large at the angles of attack of 45 and 55 deg. This is in contrast to the sharp model results where the probability of achieving low side force at these incidences is very small. The blunt and sharp model $C_{y\,peak}$ distributions are alike in that the probability of achieving a high side force level increases with increasing incidence in both cases.

IV. Discussion of Results

Repeat measurements taken at each pressure port during the LDV tests suggest that at times the vortex pattern is unsteady and may meander or jump to alternative configurations. However, it is felt that the high incidence flowfield is most aptly idealized as being steady and that variations in the side force are primarily due to changes in the mean vortex pattern. It is evident from the flowfield surveys shown in Fig. 6 that high side force levels occur when the entire visible portion of the vortex on one side of the body is shed. Smaller side force levels are associated with lower levels of flowfield asymmetry. In low side force cases the parts of the vortex pattern nearest to the model surface remain fairly symmetric. Side force measurements indicate that the magnitude of $C_{y\,peak}$ determines the level of side force along the entire body. This suggests that the initial magnitude of the flowfield asymmetry controls the degree of asymmetry along the entire model length.

The available literature on sharp, slender bodies at high incidence clearly demonstrates that side force and the associated flowfield asymmetries are roll angle dependent on axisymmetric models, regardless of the care taken in conducting the experiment and constructing the model. Thus a unique experimental description of the high angle-of-attack flowfield does not exist. It is still of practical importance to determine the side force characteristics that are repeatable. It has been suggested that the maximum observed side force can be duplicated fairly accurately.[18,19,22] This hypothesis is examined by considering the maximum observed $C_{y\,peak}$ values for the tangent ogive model with nose fineness of 3 tested during the current study. Data for a rigidly supported model of this type has been reported in Refs. 16 and 22. Also the Lamont-Hunt correlation[18] provides a prediction of maximum $C_{y\,peak}$ for such a model. The maximum observed $C_{y\,peak}$ values from these sources are given in Figs. 8-10 and in the 45-55-deg incidence range agree with one another to within 20%. When a model is tested in this incidence range at an arbitrary roll angle, the probability of attaining a $C_{y\,peak}$ nearly as large as the maximum observed value is also very high. This can be seen from the data taken during the current study which are shown in Fig. 9a. The results of Dexter and Flower[22] have been plotted in a similar manner in Fig. 10 and produce a qualitatively similar trend at an incidence of 50 deg. At an angle of attack of 35 deg the maximum observed $C_{y\,peak}$ values from these sources range from 0.5 to 1.4 and cannot be considered to agree well. The data taken in the current study and in Ref. 22 both indicate that the probability of attaining a high side force level is much smaller than it was at incidences near 50 deg. However, the probability of low side force values is much larger in the current study than in Ref. 22. Presumably the flowfield near this incidence is in the process

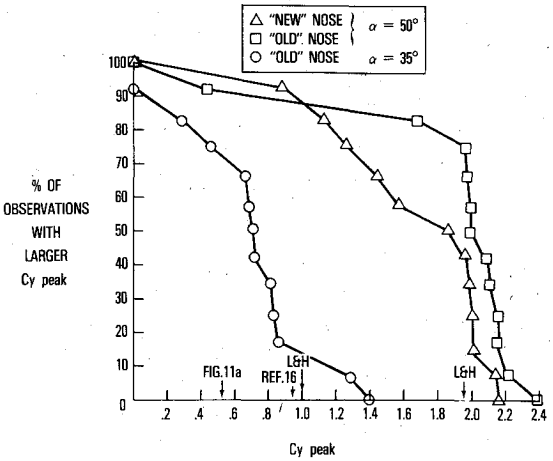

Fig. 10 $C_{y\,peak}$ as a function of the number of roll orientations producing larger values of $C_{y\,peak}$. Data is from Ref. 22. The arrows marked L&H are the maximum predicted $C_{y\,peak}$ values from the Lamont-Hunt correlation.[19]

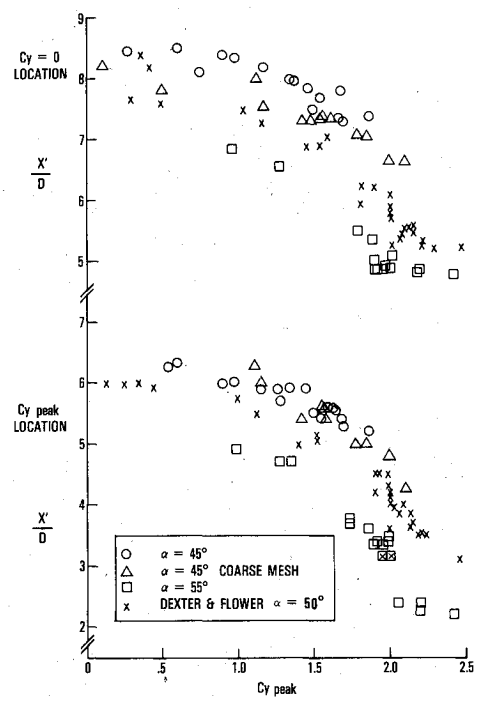

Fig. 11 Axial location of $C_{y\,peak}$ and $C_y = 0$ as a function of side force magnitude.

of changing from a symmetric to an asymmetric vortex pattern and small differences in the model construction or test facilities can have a large impact on the resultant side force.

At incidences near 45-55 deg certain characteristics of the flowfield appear reproducible in addition to the maximum $C_{y\,peak}$. In Fig. 11 the estimated location of the $C_{y\,peak}$ and the first $C_y = 0$ point have been plotted as a function of $C_{y\,peak}$ for the sharp model at $\alpha = 45$ and 55 deg. Also included in this figure are similar data from Ref. 22 that were measured at an angle of attack of 50 deg. Some of the scatter in the data taken during the current study is due to the relatively small number of instrumented cross-flow planes which made it difficult to estimate $C_{y\,peak}$ and $C_y = 0$ locations. However, results from the current study bracket those of Ref. 22 indicating that the two sets of data are consistent. This finding is important because it suggests that there is a unique flowfield associated with each side force magnitude.

V. Summary and Conclusions

Low speed wind tunnel tests have been carried out on a rigidly mounted tangent ogive model at incidences of 35, 45, and 55 deg. The measured freestream turbulence level was 0.1% and a constant streamwise Reynolds number of 1.5×10^5 was maintained throughout the study which produced a laminar boundary-layer separation. Flowfield velocities were measured using a three component LDV system and unsteady surface pressure measurements were recorded using internally mounted scanivalves and transducers. At each point in the flowfield and on the model surface 200 samples were recorded allowing the mean and standard deviations of velocities and pressures to be calculated. An analysis of the collected data leads to the following conclusions.

1) Varying side force levels are caused primarily by changes in the mean vortex pattern.

2) The highest side force values are produced by flowfields that are the most asymmetric.

3) Experiments featuring high side force levels generated lower values of σ_{c_p}.

4) The probability of obtaining a high side force level at an arbitrary model roll angle increases with increasing incidence throughout the angle-of-attack range of 35 to 55 deg.

5) The functional form of C_y is dependent on $C_{y\,\text{peak}}$ values. As $C_{y\,\text{peak}}$ decreases the distribution becomes more stretched out along the model and $C_{y\,\text{peak}}$ occurs farther from the nose. This suggests that there is a unique flowfield associated with each value of $C_{y\,\text{peak}}$.

6) Blunting the model nosetip by 10% substantially reduces side force and moves the vortices farther from the model surface. Also, the functional form of C_y appears to be independent of the value of $C_{y\,\text{peak}}$.

7) Increasing the freestream turbulence level by use of a coarse screen did not qualitatively alter the side force characteristics although it did lead to slightly higher side force levels.

Acknowledgments

This project was supported by William C. Volz of the Naval Air Systems Command. The authors wish to thank Commander Schlein and his staff at the U. S. Naval Academy for making the wind-tunnel testing facilities available. M. Szelingowski, D. Ausherman, D. Sternklar, P. Panneton, and M. E. Falusi also made significant contributions to this project.

References

[1] Clark, W. H., "Body Vortex Formation on Missiles in Incompressible Flows," AIAA Paper 77-1154, 1977.

[2] Clark, W. H. and Nelson, R. C., "Body Vortex Formation on Missiles at High Angles of Attack," AIAA Paper 76-65, 1976.

[3] Schwind, R. G. and Mullen, J., "Laser Velocimeter Measurements of Slender Body Wake Vortices," AIAA Paper 79-0302, 1979.

[4] Oberkampf, W. L., Bartel, T. J., and Martindale, W. R., "Supersonic Flow Measurements in the Body Vortex Wake of an Ogive Nose Cylinder," AIAA Paper 78-787, 1978.

[5] Oberkampf, W. L. and Bartel, T. J., "Symmetric Body Vortex Wake Characteristics in Supersonic Flow," AIAA Paper 78-1337, 1978.

[6] Mello, J. F., "Investigation of Normal Force Distribution and Wake Vortex Characteristics of Bodies of Revolution at Supersonic Speeds," *Journal of Aerospace Sciences,* Vol. 26, March 1959, pp. 155-168.

[7] Gowens, F. E. and Perkins, E. W., "Study of the Effects of Body Shape on the Vortex Wakes of Inclined Bodies at M = 2," NACA RM A53I17, 1953.

[8] Fiechter, M., "Uber Wirbelsysteme an Schlanken Rotationskorpern und Ihren Einfluss auf die Aerodynamischen Beiwerte," Deutsch-Franzosisches Forschungsinstitut, Saint-Louis, Bericht 10/66, 1966.

[9] Tingley, B. E. and Allen, C. Q., "An Investigation of the Normal Force and Vortex Wake Characteristics of an Ogive-Cylinder Body at Supersonic Speeds," NASA TN D-1207, 1962.

[10] Fidler, J. E., Schwind, R. G., and Niesen, J. N.,, "Investigations of Slender-Body Vortices," *AIAA Journal,* Vol. 15, Dec. 1977, pp. 1736-1741.

[11] Grosche, F. R., "Wind Tunnel Investigation of the Vortex System Near an Inclined Body of Revolution With and Without Wings," AGARD CP-71, Sept. 1970.

[12] Thomson, K. D. and Morrison, D. F., "The Spacing, Position and Strength of Vortices in the Wake of Slender Cylindrical Bodies at Large Incidence," *Journal of Fluid Mechanics,* Vol. 50, No. 4, 1971, pp. 751-783.

[13] Yanta, W. J. and Wardlaw, A. B., "Laser Doppler Velocimeter Measurements of Leeward Flowfields on Slender Bodies at Large Angle-of-Attack," AIAA Paper 77-660, 1977.

[14] Foley, J. E., "Results of a Study of Mach Number and Reynolds Number Effects on the Lee Side Vortex Flow Field Characteristics of an Ogive-Cylinder-Frustum-Cylinder at Angles-of-Attack to 25 Degrees," Chrysler Corp., TN-AP-72-565, 1972.

[15] Owen, F. K. and Johnson, D. A., "Wake Vortex Measurements of an Ogive Cylinder at $\alpha = 36$ Degrees," *Journal of Aircraft,* Vol. 16, Sept. 1979, pp. 577-583.

[16] Wardlaw, A. B. and Yanta, W. J., "The Flow Field About and Forces on Slender Bodies at High Incidence," AIAA Paper 80-0184, 1980.

[17] Peake, D. J., Owen, F. K., and Johnson, D. A., "Control of Forebody Vortex Orientation to Alleviate Side Forces," AIAA Paper 80-0183, 1980.

[18] Lamont, P. J. and Hunt, B. L., "Pressure and Force Distributions on a Sharp-Nosed Circular Cylinder at Large Angles of Inclination to a Uniform Subsonic Stream," *Journal of Fluid Mechanics,* Vol. 76, No. 3, 1976, pp. 519-559.

[19] Lamont, P. J. and Hunt, B. L., "Prediction of Aerodynamic Out-of-Plane Forces on Ogive-Nosed Circular Cylinders," *Journal of Spacecraft and Rockets,* Vol. 14, Jan. 1977, pp. 38-44.

[20] Yanta, W. J., "A Three Dimensional Laser Doppler Velocimeter (LDV) for Use in Wind Tunnels," International Congress on Instrumentation in Aerospace Simulation Facilities, Naval Postgraduate School, Sept. 1979.

[21] Yanta, W. J. and Wardlaw, A. B., "Multi-Stable Vortex Patterns on Slender, Circular Bodies at High Incidence," AIAA Paper 81-0006, 1981.

[22] Dexter, P. C. and Flower, J. W., "The Effects of Roll Angle on the Flow Over a Body of Revolution at High Angles of Attack," AIAA Paper 81-0358, 1981.